LAWRENCE
LIVERMORE
NATIONAL
LABORATORY

UCRL-JRNL-227199

Sub-diffraction-limited multilayer coatings for the 0.3-NA Micro-Exposure Tool for extreme ultraviolet lithography

R. Soufli, R. M. Hudyma, E. Spiller, E. M. Gullikson, M. A. Schmidt, J. C. Robinson, S. L. Baker, C. C. Walton, J. S. Taylor

January 11, 2007

Applied Optics

Updated October 14, 2003

UCRL-JRNL-227199

Sub-diffraction-limited multilayer coatings for the 0.3-NA Micro-Exposure Tool for extreme ultraviolet lithography

Regina Soufli[1], Russell M. Hudyma[2*], Eberhard Spiller[1], Eric M. Gullikson[3], Mark A. Schmidt[1], Jeff C. Robinson[1], Sherry L. Baker[1], Christopher C. Walton[1], John S. Taylor[1]

[1]Lawrence Livermore National Laboratory, 7000 East Avenue, Livermore, CA 94550

[2]Hyperion Development LLC, 358 South Overlook Drive, San Ramon, CA 94582

[3]Lawrence Berkeley National Laboratory, 1 Cyclotron Road, Berkeley, CA 94720

Abstract

This manuscript discusses the multilayer coating results for the primary and secondary mirrors of the Micro Exposure Tool (MET): a 0.30-numerical aperture (NA) lithographic imaging system with 200×600 μm^2 field of view at the wafer plane, operating in the extreme ultraviolet (EUV) wavelength region. Mo/Si multilayers were deposited by DC-magnetron sputtering on large-area, curved MET camera substrates, and a velocity modulation technique was implemented to consistently achieve multilayer thickness

[*] R. M. Hudyma was with LLNL when this work was performed.

profiles with added figure errors below 0.1 nm rms to achieve sub-diffraction-limited performance. This work represents the first experimental demonstration of sub-diffraction-limited multilayer coatings for high-NA EUV imaging systems.

1. Introduction

According to the present semiconductor industry forecast, optical technologies currently used in photolithography scanners[1] are expected in a few years to reach their limits in printing ever-smaller features. The finest resolution implemented in leading-edge logic devices is currently 65 nm and is achieved in high-volume manufacturing mode with scanners operating at illumination wavelengths of 193 nm. "Moore's law" dictates the continuous scaling of microprocessor size to smaller dimensions by requiring the doubling of computer performance approximately every 18 months. Extreme Ultraviolet Lithography (EUVL) is thought as one of the most suitable next-generation lithographic technologies for patterning features beyond the 32-nm resolution node. EUVL has been supported by the semiconductor industry[2] because it is considered the natural extension of optical lithography in the extreme ultraviolet wavelength region, it is applicable to multiple process generations, and can be cost effective for different types of semiconductor chips. In anticipation of implementing EUVL for high-volume manufacturing, the Micro-Exposure Tool (MET) has been introduced as a research-and-development system with a high numerical aperture (NA) to provide accelerated learning in key areas of interest such as photoresist development, process latitude studies, mask defect printability, and subsystem development. The MET is a micro-field (200×600 μm^2), two-mirror projection system with a NA of 0.30, and 5:1 reduction ratio. As with any reflective system operating at EUV wavelengths and near-normal incidence angles, multilayer coatings need to be deposited on optical substrates

in order to provide efficient reflectors. Two sets of Mo/Si multilayer coatings deposited for two separate MET projection systems are described in this manuscript. They are the first experimental multilayer results that meet the design specifications of a high-NA, small-field EUV camera, designed for the printing of features with resolution as fine as 20 nm. In order to meet these specifications, the requirements on thickness control during deposition of the multilayer films across the mirror surface are at a scale that is comparable to atomic dimensions. In addition to their application in the MET tool, the present results illustrate the capability to coat large optical elements for future high-NA, full-field EUV cameras for use in areas such as photolithography, astronomical instrumentation and microscopy.

2. MET specifications

2.1 Optical design

The MET two-bounce projection system is shown in Fig. 1. Two aspheric mirrors are used in a coaxial, centrally obscured configuration to achieve the NA of 0.30. One of the basic principles behind the MET design is the concept of "equal radii," wherein the radii of curvature of the primary and secondary mirrors are nearly the same (see also Table 1). This equal radii concept combined with mild aspheric correction allows for nearly perfect aberration correction of both the low and high orders of spherical aberration, coma, and particularly field curvature. For example, compared to a "10× Schwarzchild" (10:1 reduction ratio) microstepper design[3], for the same field size at the wafer, the "equal radii" concept reduces the longitudinal field curvature from 1.8 μm to less than 0.05 μm. This 36-fold reduction in field curvature broadens the range of depth of focus variations (process window) over which acceptable printing can be achieved over

the full 200×600 μm^2 field. The resulting field curvature can be corrected to a value that approaches more sophisticated, multiple-mirror, high-NA EUVL systems, thus enabling simple device patterning over a meaningful field size on the resist-coated wafer. In principle, the MET can operate in either reflection or transmission mask modes, and achieves sub-diffraction-limited imaging in both cases. As is demonstrated in Fig.1, to enable the use of a reflection mask, the mask plane is tilted at 4° to allow the illumination rays to enter the projection optics. Since the imaging is controlled by the Scheimpflug condition[4], the mask can be tilted by up to ~5°. For a 4° mask plane tilt, there is a corresponding tilt of 0.8° at the wafer plane, to allow recovery of the system nominal performance on the tilted image surface. As has been discussed in the literature[5], aberrations even smaller than the classical diffraction limit of Rayleigh (0.25 waves peak-to-valley, P-V) or Marechal (0.07 waves root-mean-square, rms) can cause appreciable changes in depth of focus and critical dimension control. Therefore, the overall wavefront error budget for the MET projection system was specified at 0.64 nm or 0.048 waves rms (assuming wavelength of illumination at 13.4 nm), which is considerably lower than the classical diffraction limit but deemed achievable given the mirror fabrication state-of-the-art at the time the MET system was designed. With a reflection mask, the "as-designed" composite wavefront error of the MET camera is 0.42 nm or 0.031 waves rms. This value is close to what is required by modern lithography projection printing optics to achieve the required resolution and critical dimension uniformity. The remaining portion of the overall MET wavefront error budget was allocated to miscellaneous system errors (alignment, mounting stress, thermal, vibration) and to substrate and multilayer fabrication, as is explained later in Section 2.2 and Section 3.

The main optical design parameters of the primary and secondary MET mirrors are outlined in Table 1. Both mirrors have mild aspheric surface profiles to correct higher-order spherical aberration and coma to lithographic standards. The radius of the best-fit sphere for each optic is given in Table 1, where the negative and positive signs signify a convex and a concave surface for the primary and secondary optic, respectively. The two mirrors follow the "equal radii" criterion as is discussed in the previous paragraph. Near the edge of the clear aperture (illuminated area) of the primary mirror the maximum aspheric slope (–1.18 μm/mm) is relatively large and was expected to present a challenge for the optical surface fabrication. For example, compared to the optics in a low-NA (NA=0.1) EUVL projection system[6,7] the maximum aspheric slope of –1.18 μm/mm of the MET primary mirror is 40% larger and approaches specifications of future high-NA, full-field EUVL camera mirrors. Table 1 shows that the ray angles of incidence on the primary mirror vary from 2.54° to 8.67° (measured from the surface normal) across the clear aperture extending from 8.4 mm to 27 mm in the radial direction. Similarly, the ray angles of incidence on the secondary mirror vary from 0.67° to 1.98° across the clear aperture extending from 11.4 mm to 91.6 mm. The variation in angle of incidence vs. mirror radius will be used later in Section 3.3 to determine the prescription for the multilayer thickness profile of each optic, and to analyze the experimental wavelength results.

2.2 Set 1 and Set 2 MET substrates

The multilayer coatings discussed in this manuscript were applied on two different sets of MET projection optics. Both sets of substrates were manufactured by Carl Zeiss (Oberkochen, Germany). Zerodur® was chosen as the substrate material, due to its favorable properties in terms

of forming a well-figured/finished surface, combined with minimum thermal distortion during manufacturing and use in the MET tool. The first set (Set 1) was produced during the developmental stage of the fabrication effort for the MET optics and was assigned a relaxed set of figure and finish specifications. A subsequent set (Set 2) incorporated the learning from the earlier fabrication of Set 1 and was assigned more advanced specifications. The substrate figure and finish properties of the two sets are summarized in Table 2. All measurement results shown in Table 2 were performed at LLNL, with the exception of the figure measurements of the MET secondary. Figure measurements at LLNL were performed by means of full-aperture, visible-light interferometry[8], covering the range of spatial periods greater than 1 mm. Mid-spatial frequency roughness (MSFR) measurements at LLNL were performed using a Zygo New View™ optical profiling microscope in the spatial period range from 1 μm to 1mm. High spatial frequency roughness (HSFR) measurements at LLNL were performed with a Digital Instruments Dimension 5000™ atomic force microscope in the spatial period range 0.02 μm to 1 μm. In the cases of MSFR and HSFR measurements, nine to twelve points within the clear aperture of each optic were averaged. The results were used to obtain the power spectral density of the surface, which was then used to determine the roughness[9] in each spatial period region, expressed in nm rms. Results obtained by the substrate manufacturer are given in Table 2 for the figure error of the secondary substrate. A complete set of measurements in the figure, mid- and high-spatial frequency ranges was also performed at the substrate manufacturer's facility[10]. A comprehensive metrology validation process took place between LLNL and the substrate manufacturer and it was concluded that measurements from the two facilities for the figure, MSFR and HSFR were in good agreement.

Figure errors contribute to wavefront distortion and degrade resolution; figure and MSFR errors are associated with flare due to scattering within the camera field of view, leading to loss of imaging contrast, as will be discussed later in this section; MSFR and HSFR cause loss of specular reflectance due to scattering outside the camera field of view[11]. All aforementioned effects can be detrimental to the imaging and throughput capabilities of a projection system and are the basic drivers behind the figure and finish specifications shown in Table 2. By comparing the results in Table 2 -for instance, the figure and MSFR results of the Set 1 primary and secondary- one may appreciate the compromises involved in simultaneously achieving surface specifications in different spatial frequency ranges. Given that the aspheric departures in Table 1 were sufficiently large to require advanced aspheric fabrication technology for both MET substrates, figuring of the primary was anticipated to incur additional difficulty due to its extremely steep aspheric slope, as is discussed earlier in Section 2.1. This fact is illustrated in Table 2 by the relatively large figure error of the primary substrate in Set 1 (0.43 nm rms), which is nevertheless greatly improved in Set 2 (0.21 nm rms). In summary, given the challenges in terms of the size, curvature and asphericity of the MET projection optics, the results shown for the Set 2 MET substrates represent the "state of the art" in aspheric surface fabrication technology at the time of manufacture of these optics.

One of the key metrics in evaluating the MET optics is the functional need for low flare, due to the high-resolution printing requirements associated with the MET camera. Flare is defined as the aerial image intensity in the center of a dark line contained in a uniformly bright field[11]. For an EUV imaging system, flare is caused by scattering from the roughness of the optics. The spatial frequency ranges of roughness associated with flare encompass the spatial frequencies

that lead to scattered light within the printed field. Spatial frequencies within the regime of figure and MSFR can lead to flare and are somewhat different for each of the MET mirrors, as listed in Table 3. Figure 2 shows calculations of flare vs. linewidth for the Set 1 and Set 2 MET substrates using the measured substrate roughness in the relevant spatial frequency bands presented in Table 3. The results demonstrate significant reduction of flare and thus improved performance of the Set 2 optics compared to Set 1, due to the improved roughness values achieved by the substrate manufacturer in the Set 2 substrates, as shown in Table 3.

3. Multilayer coatings: design and experimental results

3.1 Multilayer thickness specifications

There are several criteria that need to be met when specifying thickness tolerances for reflective, multilayer-coated optics for lithography applications[6,7,12]. All specifications discussed below apply to the illuminated area of each mirror surface (clear aperture area) in the MET camera, which is defined in Table 1.

3.1.1 Throughput

The MET is an all-reflective system with multilayer coatings on two projection elements, on a condenser/illuminator assembly (not discussed in this manuscript) and on the mask. All of these elements should be tuned to reflect at –or near- the same wavelength in order to obtain a substantial output from the camera. In a commercial, high-volume EUVL tool, a spectral mismatch between the mirrors would translate to throughput reduction. A goal was set to match the reflectance peak position of the two MET camera optics to within $\Delta\lambda = \pm 0.050$ nm, which

would ensure at least 97.4% of the throughput compared to a system with ideal wavelength-matching[13]. Although the MET is considered a research-and-development system where throughput is not a crucial requirement, the above goal was set as it would be applicable to multilayer optics for commercial, high-volume EUVL scanners. Meeting this goal requires atomic-level repeatability of the coating process from one deposition run to another. In addition to optic-to-optic wavelength matching, another throughput constraint is the tolerance on wavelength variation across the surface of any individual optic in the system. For maximum throughput, the multilayer should have its reflectivity peak at the same wavelength for all surface points on any given mirror. If an arbitrary goal is set to stay within 99% of the reflectivity peak for all points on the optic surface, then a Mo/Si multilayer operating at λ=13.4 nm is allowed to have its wavelength vary to within $\Delta\lambda = \pm$ 0.050 nm, which is equivalent to having the wavelength (or the thickness) vary from its prescribed value to within ±0.37% P-V across the surface.

3.1.2. Intensity variations

In addition to the throughput constraints discussed above, a reflectivity mismatch -or other causes such as variations in substrate roughness- across any individual mirror surface in the projection system, result in intensity variations (apodization) of the reflected wavefront at the system exit pupil. These variations can lead to a narrowing of the NA or a non-uniformity across the pupil. In lithography terms, these effects cause loss of aerial image contrast and variations in key aberrations and in the critical dimension of printed images across the field. The tolerance for these effects was determined to be ±0.2% P-V for the wavelength (or thickness) variation across each of the two MET camera optics.

3.1.3 Multilayer-added figure errors

In the spatial frequency range corresponding to surface figure, wavefront errors due to multilayer thickness variations introduce aberrations which can be detrimental to the overall performance of the imaging system. Such multilayer-induced errors can be decomposed into a compensable and a non-compensable part, the latter being the added (non-compensable) figure error that the multilayer is contributing to the system, as will also be explained in detail in Section 3.3. In order for multilayer coatings to not affect adversely the imaging system performance, their added figure errors should be negligible compared to the substrate figure error. For the MET Set 2 substrates which have the most stringent tolerances between the two sets, the figure error specification was 0.25 nm rms as is shown in Table 2. Given that the substrate and multilayer coating errors are uncorrelated, they add in a quadratic fashion. The maximum allowable added figure error due to the MET multilayer coatings was therefore set at 0.1 nm rms which for a typical 280 nm-thick Mo/Si film corresponds to 0.04% rms (~ 0.1% P-V). This multilayer-added figure error specification is consistent with sub-diffraction-limited system performance, as was explained earlier in Section 2.1.

3.1.4 Summary of multilayer tolerances for the MET mirrors

The tightest among the constraints imposed to the multilayer thickness variation in Sections 3.1.1-3.1.3, are the ±0.2% P-V thickness uniformity and the 0.1 nm rms added figure error requirements. Both of these specifications have to be met independently for a given multilayer coating: the ±0.2% P-V criterion is applied to the as-measured multilayer thickness profile, while the added figure error is determined from the non-compensable portion of the as-measured profile, as will be explained in Section 3.3. Satisfying the 0.1 nm rms added figure error constraint depends to a large degree on the "shape" of the thickness profile, i.e. profile shapes

approaching a 2nd order polynomial are largely compensable during system alignment. During process development of the MET multilayer coatings and by testing of various experimental profiles, it was concluded that the 0.1 nm rms added figure error tolerance requires the tightest control on the coating thickness. For this reason, the thickness profiles presented in Section 3.3 have been optimized primarily for lowest added figure error, rather than P-V uniformity.

The next generation of EUVL projection optics will be implemented in beta and production tools. Substrate figure requirements have been set at about 0.1 nm rms for these systems. Consequently, multilayer-added figure errors of less than 0.05 nm rms should be achieved, a factor of 2 more stringent than the MET camera requirements. Commercial EUVL scanner designs include six-mirror cameras, with the clear aperture extending up to 200 mm from the optical axis, for some of the mirrors. In order to meet all the additional constraints imposed on EUVL beta and production multilayer coatings, extremely sophisticated control of the multilayer film thickness will be required. The results presented in Section 3.3 illustrate the feasibility of meeting such specifications.

3.2 Experimental setup

The MET Set 1 and Set 2 coatings were deposited using a large-scale DC-magnetron deposition system shown in Fig. 3 (a), which has been described in detail previously[9]. The system chamber has a sputter-down configuration, five-target capability, and can accommodate four optical substrates of up to 470 mm in diameter, or fewer substrates of up to 600 mm in diameter. The chamber size and geometry enable coating of the primary and secondary mirror of each MET set in a single deposition run. Substrates were mounted on a platter rotating at speeds of the order of

1 rpm during deposition, which passes alternately under the Si and Mo targets. In addition to the platter motion, each optic is also spun at 400 rpm around its optical axis (which, in the case of the MET mirrors coincides with the geometric center of the optic surface), to average out possible non-uniformities across the surface area of the target materials. Base pressure was maintained at 3×10^{-8} Torr during the actual MET deposition runs, and the process gas (Ar) pressure was 10^{-3} Torr. The Si and Mo targets were operated at powers of 2500 and 1000 Watts, respectively. Typical reflectance results from this deposition system are illustrated in Fig. 3(b), where measured EUV reflectivities from multilayer coatings with N=40 and N=60 Mo/Si bi-layer pairs on Si wafer substrates are shown. Since high throughput is not of critical importance for the low-power MET camera compared to other requirements such as low wavefront error, a modest number of bi-layers (N=40) was applied in both Set 1 and Set 2 of MET coatings. In this manner, reasonably high reflectance is ensured while the multilayer-added figure error is kept as low as possible (see also discussion in Sections 3.1, 3.3). The ratio of Mo thickness in the Mo/Si bilayer of the MET coatings was Γ=0.4 and the stack of N=40 Mo/Si pairs was finished with a Si capping layer in both MET sets. For multilayer coatings operating at near-normal angles of incidence in the wavelength region just longer than the Si $L_{2,3}$ absorption edge (12.4 nm) shown in Figure 3 (b), a bi-layer thickness of about 7 nm and N=40 bi-layers result in a total multilayer film thickness of about 280 nm. All EUV reflectance measurements described in this manuscript were performed at Beamline 6.3.2 of the Advanced Light Source (ALS) synchrotron at Lawrence Berkeley National Laboratory[14]. A Si photodiode detector with acceptance angle of 2.4° was used in all EUV reflectance measurements. The beamline reflectometer is capable of delivering EUV wavelength and reflectance results with 0.007% and 0.08% relative precision, respectively.

Among the key elements towards meeting stringent multilayer thickness specifications on large-area, curved optics is the velocity modulation method[15], outlined in Fig. 4. This method has been used previously[6,7] to successfully coat multilayer optics for low-NA systems, and it is being demonstrated on larger-area, high-NA optics in the present manuscript. Prior to deposition, a computer model is employed simulating the deposition process inside the chamber and taking into account all relevant parameters, including the tilt and sag at each point of the optic surface in the case of curved substrates. For a given goal multilayer thickness profile (uniform or graded), the output parameters of this model are: (i) the ratio(s) among deposition platter velocities and (ii) the corresponding platter angle(s) where the aforementioned velocities need to be applied as the substrate is passing under each sputtering target. The elements in (i), (ii) define the normalized multilayer thickness profile which is needed to determine the multilayer-added figure error, the most crucial among all multilayer specifications discussed in Section 3.1, and later in Section 3.3. Optimization of (i) and (ii) to meet the added figure error requirements is thus the most challenging step during multilayer process development. The output of the velocity modulation model is implemented in a first experimental deposition run, which takes place on an inexpensive test optic. The test optic is a spherical approximation of the actual mirror that will ultimately be coated, with significantly relaxed figure and finish tolerances. Such test optics can usually be obtained from the manufacturer at relatively low cost. After the first test deposition run is performed, the resulting thickness profile is determined by means of EUV reflectance measurements. The results are evaluated and corrections to the platter velocities/angles are applied in the next test deposition run. This routine is repeated until a multilayer coating is reached that meets the required specifications in terms of multilayer-added figure error and wavelength, as verified by EUV reflectance measurements. The technique described above for

multilayer thickness control is robust, rapidly converging, and as will also be shown in the next Section, it has consistently produced multilayer coatings with atomic-scale precision. This method allows the thickness of each coating to be controlled independently as each substrate is passing under each sputtering target. Therefore, multiple optics requiring different thickness profiles (and thus different coating algorithms) can be optimized and ultimately coated during the same deposition run, as is the case with the MET primary and secondary mirrors. The desired thickness profile for the MET primary was reached after six coating iterations, and the MET secondary mirror required two additional (i.e. a total of eight) iterations. These are representative process development lengths, with larger area optics generally requiring a larger number of test coating runs until thickness profile specifications are met across the entire clear aperture.

3.3 Multilayer coating results and discussion

To achieve reflectance at a constant wavelength across the illuminated surface of each mirror, the as-designed thickness profiles for both primary and secondary are graded according to the variation in angles of incidence for each mirror discussed in Section 2.1. EUV reflectance vs. wavelength was measured on several points across the surface of each mirror at a fixed angle of incidence, θ_m. The MET primary was measured at $\theta_m = 5.5°$ and the MET secondary was measured at $\theta_m = 3°$, both defined from the direction normal to the surface. By measuring the wavelength λ at a fixed angle θ_m across the optic surface, it is quite straightforward to derive the coating thickness variation across the surface as is shown in eq. (2) since multilayer wavelength and thickness are proportional according to the Bragg condition. The thickness profiles of the MET Set 2 coatings measured in this manner are shown in Fig. 5. The multilayer-added figure error is extracted from these results after subtracting the portion of thickness variation that can be compensated during alignment of the actual MET system. The compensable portion is

represented by a best-fit spherical term, which can be aligned out through tilt and focus shifts after the mirrors are installed in the MET camera. For this reason, during process development where different coating algorithms and profile results are evaluated for each MET optic, the most desirable thickness profiles are the most compensable, i.e: the families of profile curves with spherical-like shapes[6]. The remainder of the subtraction (non-compensable portion of multilayer thickness variation) is the multilayer-added figure error, with its value weighted according to illuminated area, and is plotted at the lower part of the graphs in Fig. 5. In all Set 1 and Set 2 MET coatings, multilayer-added figure errors of about 0.06 nm rms were achieved, well within the specification of 0.1 nm rms discussed in Sections 3.1.3, 3.1.4. The Set 2 coatings were performed 11 months after the Set 1 coatings using identical velocity modulation algorithms, with the deposition system continuously operating in the meantime. The measured thickness profiles for the Set 1 and Set 2 MET coatings are plotted in Fig. 6.

To confirm the effect of the multilayer coatings in the MET system performance, the wavefront error of the 2-bounce projection system was analyzed before and after multilayer coating. The analysis was performed by simulating[16] the wavefront error of the as-designed system assuming perfect multilayer coating profiles and then decomposing the resulting optical path difference map in terms of the fringe Zernike polynomials[17,18]. The analysis was repeated by applying the measured multilayer thickness profiles to the system model. This method captures the multilayer-induced optical path difference error. The fringe Zernike decomposition is used because it is the standard wavefront representation in commercially available lithographic simulation codes. To enable a continuous pupil domain required for the fringe Zernike decomposition, the wavefront error map in both cases was computed numerically across the exit

pupil including the central obscuration region. Table 4a illustrates the term-by-term difference in fringe Zernike decomposition in the case of an ideal multilayer coating versus the measured multilayer coating for the axial field point. Table 4b summarizes the rms wavefront error for 8 field points, including the axial field point, across the 600 μm x 200 μm field. For the axial field point, the rms wavefront error of the system is shown to be 0.024 waves. After applying the experimental results, the resulting rms wavefront of the system at this same axial field point increases to 0.034 waves. If this analysis is performed across the entire 600 μm x 200 μm printing field, then the average added wavefront error value becomes 0.006 waves (0.081 nm) rms across the field. If the individual non-compensable errors of Figure 5 are used to compute the added wavefront error, then the result is 0.165 nm rms. The difference between these two values is due to the fact that the 0.081 nm value is generated by refocusing the image plane of the system to minimize the field-composite rms wavefront error, taking advantage of the fact that defocus can be used to minimize the resulting aberration residual induced by the multilayer coatings across the field. Our estimate in Figure 5 is an approximation that does not take into account this compensating effect and uses only the axial field point. This level of multilayer-induced wavefront error is insignificant given the substrate figure of the MET projection system, which dominates the as-built wavefront error. This fact was taken into account during the optimization process of the multilayer profiles discussed in Section 3.2. Although further reduction of the multilayer-added figure errors could have been achieved with additional coating iterations during process development, ultimately it would not have made any difference in the system performance. Therefore, the multilayer optimization was completed when the multilayer-added figure errors reached values below 0.1 nm rms, which rendered them “invisible” compared to the substrate figure errors.

The design wavelength for the Set 1 MET coatings was set at 13.352 nm; the aim was to match the wavelength of the 0.1-NA, four-mirror EUVL camera[6], in case exposures had to be performed in both systems and compared side-by-side. The Set 2 MET camera was planned for use with a laser-produced Xe plasma illumination source whose spectrum peaked at a centroid wavelength of 13.500 nm, therefore this value was used as the goal wavelength for the Set 2 MET coatings. Since both primary and secondary mirrors have varied angles of incidence across their surface (see Table 1), the multilayer coating wavelength at each point is evaluated at the actual MET camera angles of incidence for that mirror and ideally it should remain constant across the surface and match the value that was set as the goal. For the MET primary, measured at fixed angle of incidence θ_m=5.5° and operating at 2.54°< θ_i <8.67° across the clear aperture 8.4 mm < r < 27 mm (Table 1), θ_m matches θ_i at r =17.75 mm. Due to geometrical constraints inside the ALS reflectometer chamber, the MET secondary had to be measured at θ_m=3° which does not match the actual angles of incidence 0.67°<θ_i<1.98° at any point within the clear aperture 11.4 mm < r <91.6 mm. Since θ_m is sufficiently close to θ_i and near the normal incidence direction for each mirror, the wavelength λ_i at the actual MET angles of operation can be translated from the EUV reflectance measurements at fixed angle of incidence θ_m, through the modified Bragg relation:

$$\lambda_i=\lambda_m (A_i/ A_m) \cos\theta_i / \cos\theta_m \qquad (2)$$

where $A_i = (1-2\delta/\cos^2\theta_i)^{1/2}$, $A_m = (1-2\delta/\cos^2\theta_m)^{1/2}$, $\delta = \sum d_j\delta_j / \sum d_j$, (j=1 for Mo, j=2 for Si), d_j is the thickness and $n_j=1- \delta_j + i* \beta_j$ is the complex refractive index of each constituent material in the bilayer[19]. Equation (2) is applied within the approximation that the wavelengths λ_i, λ_m are

close enough so that the same δ can be used at both wavelengths. The experimental results for the Set 1 and Set 2 MET multilayer coatings after the wavelengths have been translated to the actual MET camera angles of incidence according to Eq. (2), are plotted in Fig. 7. In both Set 1 and Set 2 camera optics, ideal optic-to-optic wavelength matching is achieved, and the goal wavelength is met within 0.007 nm for Set 1 and exactly for Set 2, well within the specifications stated in Section 3.1.1. The wavelength uniformity across each mirror surface meets the ±0.2% P-V requirement discussed in Section 3.1.2. The fact that both camera mirrors of each set were coated in the same deposition run minimized possible wavelength drifts that could have occurred if the optics had to be coated in two different deposition runs and thus contributed to the ideal optic-to-optic wavelength matching demonstrated in Fig. 7.

The peak reflectance of the MET mirrors was measured near the center of the clear aperture of each optic at 58% (Set 1 primary), 62.5 % (Set 1 secondary), 61.2% (Set 2 primary) and 62.4 % (Set 2 secondary) he variation in reflectance values among the four mirrors is consistent with the high spatial frequency roughness values of the substrates given in Tables 2 and 4, measured by atomic force microscopy of the substrates prior to multilayer coating, and is also consistent with scattering measurements of the coated optics performed at the ALS. The angular distribution of non-specularly scattered light was measured for the Set 1 and Set 2 secondary mirrors. Measurements were performed at the nominal angle of incidence of each of the mirrors in the MET camera, at the peak wavelength previously determined from the EUV reflectance measurements discussed earlier in this Section. Scattering results from the Set 2 secondary mirror are shown in Figure 8. The experimental data are in excellent agreement with the predicted distribution. The predicted distribution was calculated with the distorted wave Born

approximation[20] using the measured PSD of the substrate. The effect of the multilayer was included using a linear growth model[21]. For scattering angles below about 6 degrees the angular distribution is proportional to the PSD. For angles larger than 6 degrees the scattering drops off faster than the PSD since light scattered from the individual interfaces within the multilayer no longer adds in phase. EUV light scattered out of the detector is seen as a reduced reflectance when the mirrors are measured on the reflectometer. The reflectance loss due to scattering was calculated from the measured PSDs of the substrates and the predicted loss for each of the four mirrors is given in Table 5. If the predicted loss due to scattering is added to the measured reflectivity for each of the mirrors the result is within 1% of the reflectance obtained on a smooth Si wafer. This provides confirmation that the reduced reflectivity measured on these mirrors is a result of scattering due to substrate roughness. The non-specular scattering measurements for each of the mirrors provide an important verification of the surface PSD characterization and demonstrates the ability to predict the reflectance loss of a multilayer deposited on a rough substrate.

Conclusions

The first experimental demonstration of multilayer coatings for a sub-diffraction-limited, 0.3-NA camera operating in the EUV wavelength region has been presented in this manuscript. Two sets of actual MET camera mirrors were coated with Mo/Si multilayer films, and all coatings achieved sub-diffraction limited performance. The Set 2 coated mirrors were assembled into the MET camera at LLNL and were installed at beamline 12.0.1 of the ALS (LBNL). After at-wavelength alignment, wavefront quality of 0.55 nm rms (λ_{EUV} / 24.5) was demonstrated[22]. EUV exposures performed with the Set 2 MET camera at the ALS demonstrated printing of 25 nm equal line-space features, and 29 nm isolated-line features with line-edge roughness approaching

3 nm, limited by the availability of high-resolution photoresists[23]. The Set 2 MET camera remains the highest-resolution micro-field imaging tool operating to date at EUV wavelengths.

Acknowledgements

The authors are thankful to Susan Ratti, Rick Levesque, and Jay Ayers (LLNL) for engineering assistance, Ben Kaufmann and Andy Aquila (LBNL) for assistance with the EUV reflectance measurements, Ken Goldberg and Patrick Naulleau (LBNL) for enlightening discussions. The contributions and support of Claude Montcalm (formerly with LLNL, now with Xenocs, France), Jim Folta, Don Sweeney, Michael A. Johnson, Don Phillion and the late Gary Sommargren (LLNL), are greatly appreciated. We gratefully acknowledge helpful interactions with staff members at Carl Zeiss.

This work was performed under the auspices of the U.S. Department of Energy by the University of California Lawrence Livermore National Laboratory under Contract No. W-7405-ENG-48. Funding was provided by Sematech. Additional support was provided by the Extreme Ultraviolet Limited Liability Company (EUV LLC).

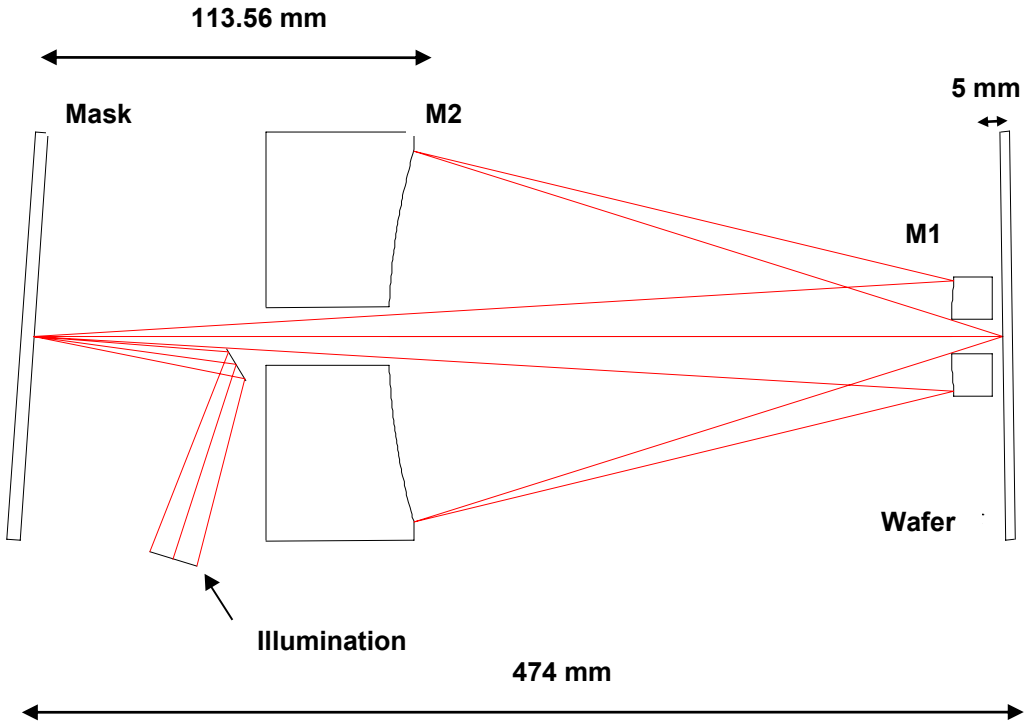

Figure 1: Schematic diagram of the MET camera, showing the marginal ray path through the reflective mask, the primary (M1) and secondary (M2) mirrors, and the wafer. Two baffles -not shown in this drawing- are also placed near the optical axis of the system, in order to block the incident beam from reaching the wafer.

	MET primary	MET secondary
Best-fit sphere radius (mm)	**- 312.63 (convex)**	**340.05 (concave)**
Peak aspheric departure (μm)	**3.82**	**5.61**
Maximum aspheric slope (μm/mm)	**- 1.18**	**- 0.47**
Clear aperture radius (mm)	**8.4 - 27**	**11.4 - 91.6**
Range of incidence angles	**2.54°- 8.67°**	**0.67°-1.98°**

Table 1: List of optical design parameters for the MET two-mirror camera.

	SET 1			SET 2		
	Figure	**MSFR**	**HSFR**	**Figure**	**MSFR**	**HSFR**
MET primary	**0.43**	**0.33**	**0.54**	**0.22**	**0.25**	**0.38**
MET secondary	**0.25**[α]	**0.46**	**0.38**	**0.21**[α]	**0.28**	**0.37**
Specifications	***0.33***	***0.30***	***0.50***	***0.25***	***0.20***	***0.4***

[α] Measured at Carl Zeiss, Oberkochen, Germany. See also Ref. 10.

Table 2: Metrology results for the roughness in the low (figure), mid (MSFR) and high (HSFR) spatial frequencies for two sets of MET substrates are shown with their respective specifications. All numbers are given in units of nm rms.

	Spatial frequency range relevant to flare	Substrate roughness (nm rms)	
		Set 1	Set 2
MET primary	0.11-160 mm^{-1}	0.43	0.27
MET secondary	0.031-50 mm^{-1}	0.35	0.20

Table 3: Spatial frequency ranges relevant to flare in the MET optical system and the roughness achieved in these bands by the manufacturer of the Set 1 and Set 2 substrates.

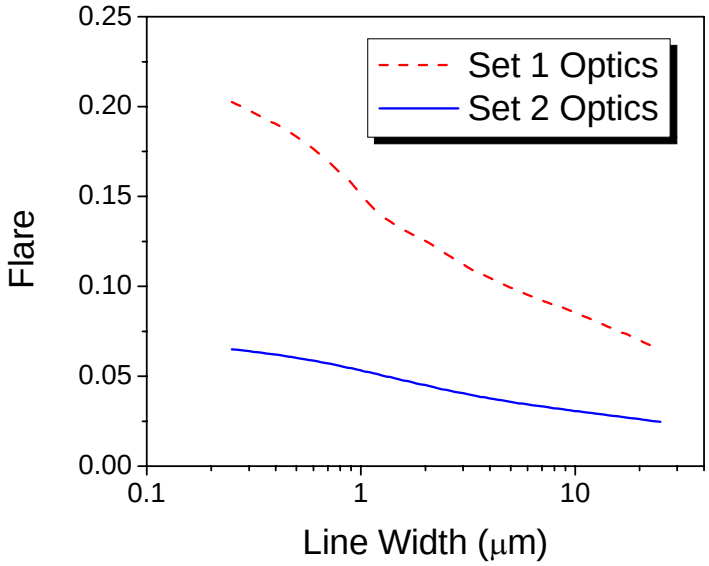

Figure 2: The calculated flare versus line width for cameras using the Set 1 and Set 2 optics.

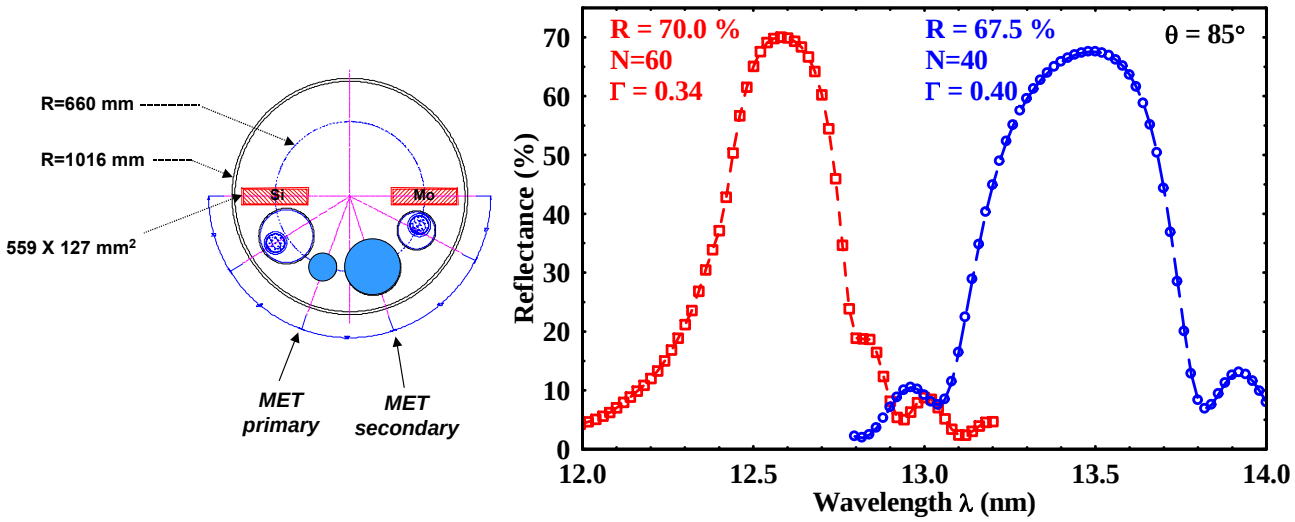

(a) **(b)**

Figure 3: (a) Schematic diagram of the DC-magnetron deposition system used to coat the MET optics. The two substrate positions holding the MET optics are shown. **(b)** Typical experimental reflectance vs. wavelength results obtained from two Mo/Si multilayers deposited in the system, measured at 5° off-normal incidence angles. The peak reflectance (R), number of bi-layers (N) and ratio of Mo in the Mo/Si bi-layer (Γ) is also noted next to each measurement. In order to demonstrate the reflective properties of the films, substrates with almost ideally smooth surfaces (Si wafers, HSFR ≤ 0.1 nm) were used, as determined by atomic force microscopy.

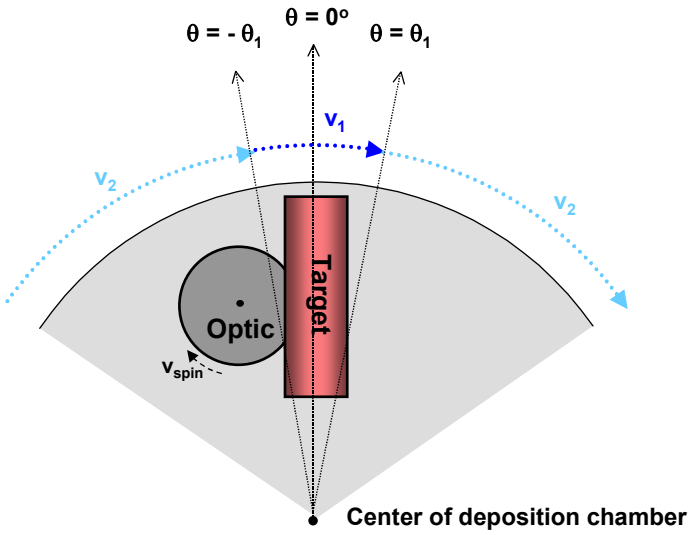

Figure 4: Schematic drawing of a section of the deposition chamber (top view), showing the motion of an optical substrate mounted on the platter, as it travels under the sputtering target. In the two-velocity scenario shown here, the ratio of velocities v_2/v_1 and the angle θ_1 where v_2 transitions to v_1 (and vice versa) determine the multilayer thickness profile deposited on the surface. The system allows for a maximum of five different velocities across the optic.

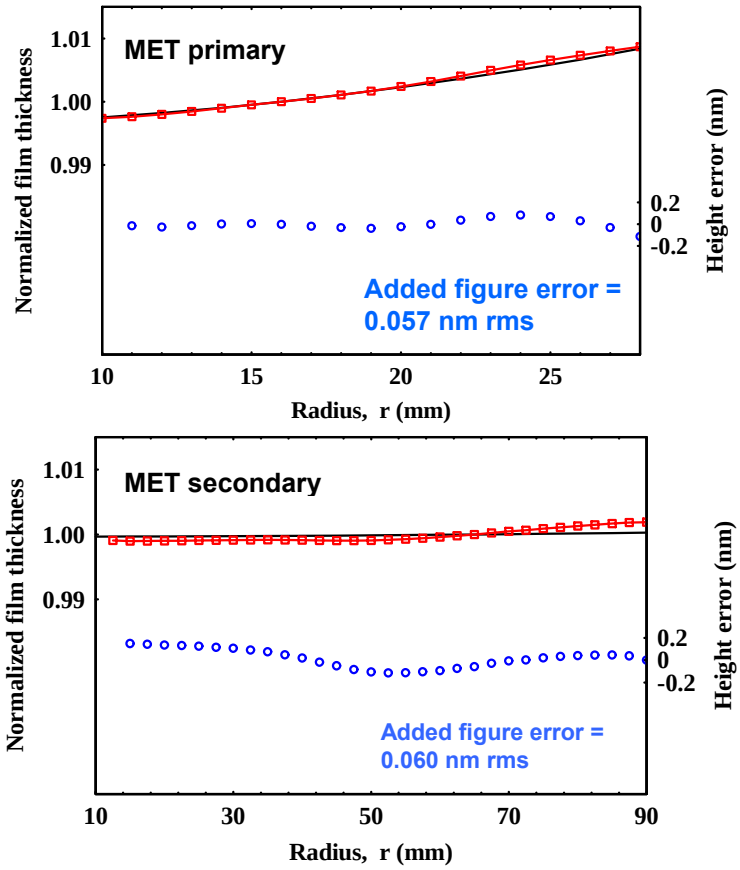

Figure 5: Measured multilayer thickness results are plotted vs. radial distance from the optical axis for the primary and secondary MET Set 2 mirrors. The clear aperture area of each optic is shown. In each plot, the top 2 curves (left y-axis) are: the measured thickness profile (square data points) and the design thickness profile (solid line). Each data point is derived from the wavelength at the center of the full-width-at-half-maximum of the measured EUV reflectance Bragg peak. Data have been normalized to the wavelength at an arbitrary location on the surface. The bottom curve (circle data points plotted on the right y-axis) represents the non-compensable figure error that the Mo/Si multilayer film is adding to the optic surface. Both primary and secondary multilayer coatings contribute added figure errors well within the 0.1 nm rms specification.

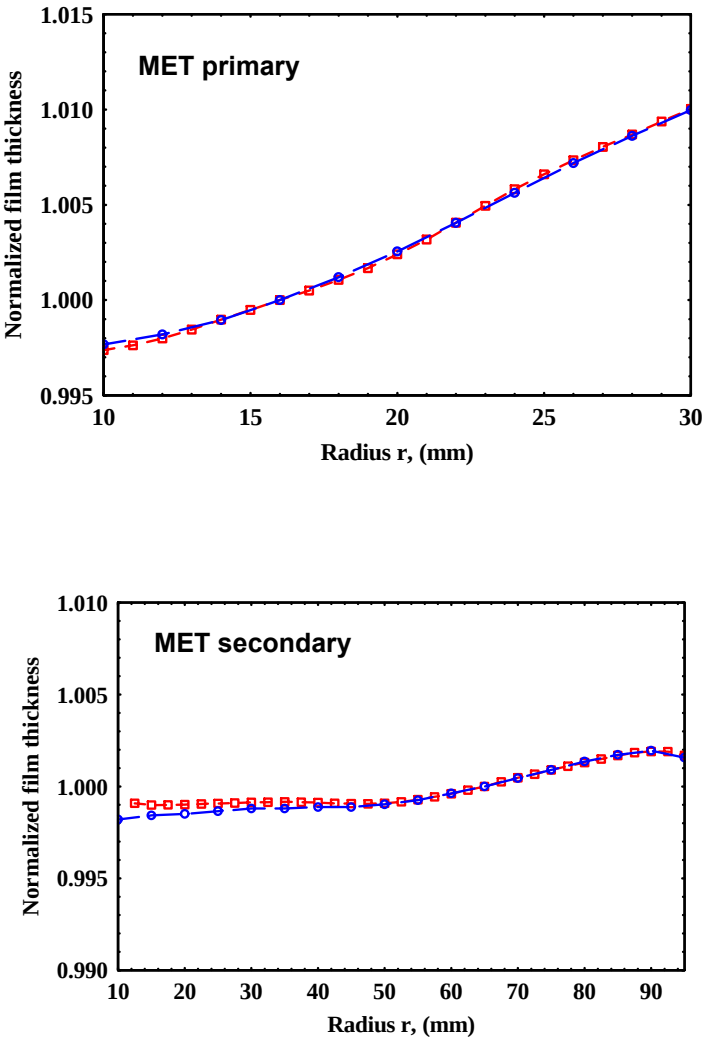

Figure 6: Measured multilayer thickness profiles are shown for the primary and secondary MET mirrors. Results from two sets of MET optics (Set 1 = squares, Set 2 = circles) are plotted, with the two coating sets performed 11 months apart, using identical velocity modulation parameters. The agreement between Set 1 and Set 2 results indicates excellent reproducibility of the deposition process.

Term	Description	F1 (Ideal)	F1 (Experimental)	Term by term difference
Z1	piston	-0.0332	-0.0963	0.0631
Z2	x-tilt	0.0000	0.0000	0.0000
Z3	y-tilt	0.0002	0.0003	-0.0002
Z4	focus	-0.0404	-0.0521	0.0117
Z5	astigmatism (0 deg/90 deg)	0.0001	0.0003	-0.0002
Z6	astigmatism (+/- 45 deg)	0.0000	0.0000	0.0000
Z7	x-coma	0.0000	0.0000	0.0000
Z8	y-coma	0.0000	0.0004	-0.0004
Z9	3rd-order spherical	0.0105	0.0290	-0.0185
Z10	trifoil	0.0000	0.0000	0.0000
Z11	trifoil	0.0000	0.0000	0.0000
Z12	5th-order astigmatism	-0.0001	0.0002	-0.0003
Z13	5th-order astigmatism	0.0000	0.0000	0.0000
Z14	5th-order coma	0.0000	0.0000	0.0000
Z15	5th-order coma	0.0001	0.0006	-0.0005
Z16	5th-order spherical	0.0098	-0.0233	0.0331
Z25	7th-order spherical	-0.0094	-0.0096	0.0002
Z36	9th-order spherical	-0.0018	-0.0018	0.0000
	RMS Wavefront error	0.024	0.034	0.010

Table 4a: A decomposition of the MET system wavefront error in fringe Zernike polynomial terms is computed for the cases of ideal and experimental multilayer coatings at the central field point (F1).

Field point	X (μm)	Y (μm)	WFE (nm rms) Uncoated	WFE (nm rms) Coated	Difference (nm rms)
F1	0.00	0.00	0.024	0.034	0.010
F2	0.00	100.00	0.048	0.055	0.007
F3	300.00	100.00	0.019	0.028	0.009
F4	300.00	0.00	0.024	0.027	0.003
F5	300.00	-100.00	0.055	0.053	-0.002
F6	0.00	-100.00	0.017	0.024	0.007
F7	210.00	-70.00	0.024	0.027	0.003
F8	210.00	70.00	0.024	0.033	0.009
				Average =	0.006

Table 4b: The rms wavefront error (WFE) is computed at eight points (F1-F8) across the MET field, for the cases of ideal and experimental multilayer coatings.

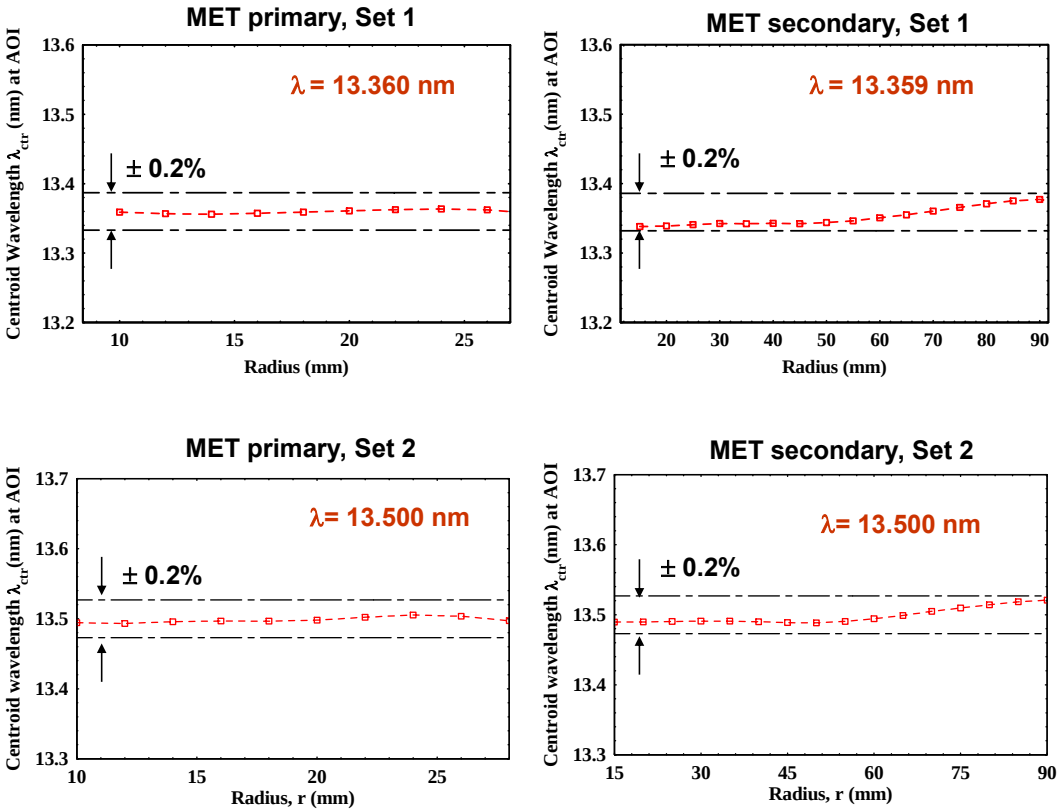

Figure 7: Experimental results for the Mo/Si wavelength vs. radius across each MET mirror, corresponding to the actual camera angles of incidence. The average wavelength is noted on the top right corner of each plot. The dash guidelines in each plot represent the ±0.2% P-V wavelength uniformity specification discussed in Section 3.1.2. The goal wavelength was 13.352 nm for the multilayer coatings in Set 1 and 13.500 nm for Set 2.

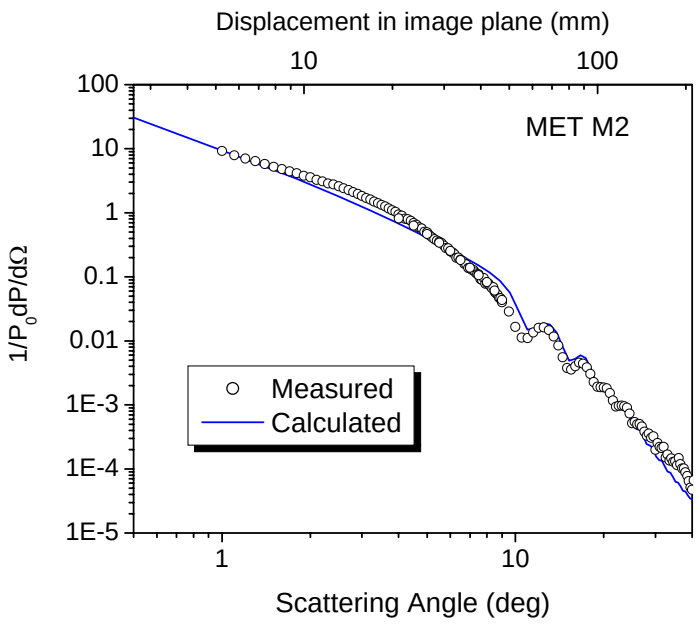

Figure 8: The angular distribution of scattering measured for the secondary mirror of the MET Set 2 optics. The calculated distribution is obtained using the distorted wave Born approximation and the measured PSD of the surface.

	SET 1		SET 2	
	Primary	**Secondary**	**Primary**	**Secondary**
Substrate HSFR (nm rms)	**0.54**	**0.38**	**0.38**	**0.37**
Predicted loss ΔR	**10.5%**	**5.5%**	**6.1%**	**5.2%**
Measured R	**58%**	**62.5%**	**61.2%**	**62.4%**
R + ΔR	**68.5%**	**68%**	**67.3%**	**67.6%**

Table 5: HSFR of the MET substrates measured by atomic force microscopy, the calculated EUV reflectance loss (ΔR, given in absolute %) due to light scattered outside of the detector acceptance angle in the reflectometer, and measured peak EUV reflectance (R). The sum of R and ΔR is consistent within 1% with the experimental Mo/Si reflectance (N=40, Γ = 0.4) on an ideally smooth substrate shown in Figure 3(b), thus demonstrating consistency between all aforementioned results.

References

[1] A "scanner" is a semiconductor industry term for tools used to print microprocessor circuit patterns, typically in "step-and-scan" mode.

[2] C. W. Gwyn, R. Stulen, D. Sweeney, and D. Attwood, "Extreme ultraviolet lithography," J. Vac. Sci. Technol. B **16**, 3142- 3149 (1998).

[3] C. Montcalm, E. Spiller, F. J. Weber, M. Wedowski, and J. A. Folta, "Multilayer coating and test of the optics for two new 10X Microstepper extreme-ultraviolet lithography cameras", J. Vac. Sci. Technol. B **19**(4), 1219-1228 (2001).

[4] The Scheimpflug condition states that the imaging properties of a centered optical system with a tilted object are preserved on a tilted image plane (ignoring distortion). For a system used at finite conjugates, the required image plane tilt is the object plane tilt scaled by the reduction ratio.

[5] D. M. Williamson, "The Elusive Diffraction Limit", OSA Proceedings on *Extreme Ultraviolet Lithography* Vol. 23, F. Zernike and D. T. Attwood (eds.), (Optical Society of America, Washington, DC, 1994), pp. 68-76.

[6] R. Soufli, E. Spiller, M. A. Schmidt, J. C. Davidson, R. F. Grabner, E. M. Gullikson, B. B. Kaufmann, S. L. Baker, H. N. Chapman, R. M. Hudyma, J. S. Taylor, C. C. Walton, C. Montcalm, and J. A. Folta, "Multilayer optics for an extreme ultraviolet lithography tool with 70 nm resolution," in *Emerging Lithographic Technologies V,* E. A. Dobisz ed., Proc. SPIE **4343**, 51-59 (2001).

[7] C. Montcalm, R. F. Grabner, R. M. Hudyma, M. A. Schmidt, E. Spiller, C. C. Walton, M. Wedowski, and J. A. Folta, "Atomic-precision multilayer coating of the first set of optics for an extreme-ultraviolet lithography prototype system", Appl. Opt. **41**, 3262-3269 (2002).

[8] Sommargren, G.E., "Phase shifting diffraction interferometry for measuring extreme ultraviolet optics," OSA Trends in Optics and Photonics Vol. 4, *Extreme Ultraviolet Lithography*, G. Kubiak and D. Kania, eds. (Optical Society of America, Washington, DC 1996), pp. 108-112.

[9] R. Soufli, E. Spiller, M. A. Schmidt, J. C. Robinson, S. L. Baker, S. Ratti, M. A. Johnson and E. M. Gullikson, "Smoothing of diamond-turned substrates for extreme-ultraviolet illuminators", Opt. Eng. **43**(12), 3089-3095 (2004).

[10] U. Dinger, G. Seitz, S. Schulte, F. Eisert, C. Münster, S. Burkhart, S. Stacklies, C. Bustaus, H. Höfer, M. Mayer, B. Fellner, O. Hocky, M. Rupp, K. Riedelsheimer, P. Kürz, "Fabrication and metrology of diffraction-limited soft x-ray optics for the EUV microlithography", in *Advances in Mirror Technology for X-Ray, EUV Lithography, Laser, and Other Applications*, A. M. Khounsary, U. Dinger and K. Ota (eds.), Proceedings of SPIE **5193**, 18-28 (2004).

[11] E.M. Gullikson, S. L. Baker, J. E. Bjorkholm, J. Bokor, K. A. Goldberg, J. E. M. Goldsmith, C. Montcalm, P. Naulleau, E. Spiller, D. G. Stearns, J. S. Taylor, J. H. Underwood, "EUV scattering and flare of 10x projection cameras", in *Emerging Lithographic Technologies III*, Y. Vladimirski, Ed.,Proceedings of SPIE **3676**, 717-723 (1999).

[12] D. W. Sweeney, R. M. Hudyma, H. N. Chapman, D. Shafer, "EUV optical design for a 100 nm CD imaging system," in *Emerging Lithographic Technologies II,* Y. Vladimirski, Ed., Proceedings of SPIE **3331**, 2-10 (1998).

[13] For this throughput calculation a total of six reflections were assumed in the MET system, including: the mask, the two MET camera optics, and a condenser/illuminator assembly with three elements. Since there was no definite MET condenser design available when this manuscript was prepared, the choice of number of condenser elements is somewhat arbitrary, but realistic.

[14] E. M. Gullikson, S. Mrowka, and B. B. Kaufmann, "Recent developments in EUV reflectometry at the Advanced Light Source," in *Emerging Lithographic Technologies V,* E. A. Dobisz ed., Proc. SPIE **4343**, 363-373 (2001).

[15] C. Montcalm, C. C. Walton, J. A. Folta, "Method and system using power modulation and velocity modulation producing sputtered thin films with sub-angstrom thickness uniformity or custom thickness gradients", U.S. Patent No. 6,668,207.

[16] Code V® software, by Optical Research Associates, Pasadena, California.

[17] F. Zernike, "Beugungstheorie des Schneidenverfahrens und seiner verbesserten Form, der Phasenkontrastmethode", Physica **1**, 689-704 (1934).

[18] J. C. Wyant and K. Creath, *"Applied optics and optical engineering",* Volume 11, New York, Academic Press, 1992.

[19] E. Spiller, "Soft X-ray Optics", SPIE Optical Engineering Press, Bellingham, WA (1994).

[20] V. Holy and T. Baumbach, "Non-specular x-ray reflection from rough multilayers," Phys. Rev. B **49**, 10668-76 (1994).

[21] D. G. Stearns, "Stochastic model for thin film growth and erosion," Appl. Phys. Lett. **62**, 1745-7 (1993).

[22] K. A. Goldberg, P. P. Naulleau, P. E. Denham, S. B. Rekawa, K. Jackson, E. H. Anderson, and J. A. Liddle, "At-wavelength alignment and testing of the 0.3-NA MET optic", J. Vac. Sci. Technol. B **22**(6), 2956-2961 (2005).

[23] P. P. Naulleau, K. A. Goldberg, J. P. Cain, E. H. Anderson, P. Denham, B. Hoef, K. Jackson, A.-S. Morlens, S. Rekawa, K. Dean, "EUV microexposures at the ALS using the 0.3-NA MET projection optics," Proc. SPIE **5751**, 56-63 (2005).